scientific reports

OPEN

Real-time assessment of PV-DSTATCOM for grid power quality enhancement using an indirect current control strategy

Vinamra Kumar Govil[1✉], S. M. Tripathi[2] & Kuldeep Sahay[3]

This paper presents a real-time simulation of a photovoltaic-based distribution static compensator (PV-DSTATCOM) using the Typhoon HIL 604 simulator, demonstrating its effectiveness in reactive power compensation, harmonic mitigation, and active power injection. The system seamlessly transitions between pure DSTATCOM mode, operating during night-time or when PV generation is zero, and PV-DSTATCOM mode, where it injects PV power while enhancing the power quality. A voltage source converter (VSC) regulated by an indirect current control strategy ensures improved power quality at the point of common coupling (PCC). Real-time simulation results under both balanced and unbalanced PCC voltage conditions validate the ability of the PV-DSTATCOM to mitigate power quality disturbances. Notably, the PV-DSTATCOM effectively reduces total harmonic distortion (THD), maintaining levels between 3.03%–5.58% under balanced PCC voltage and 3.95%–5.93% under unbalanced PCC voltage conditions, generally adhering to or remaining near the acceptable limit of IEEE-519 standards across varying solar irradiance levels and non-linear load conditions. Additionally, it maintains a near-unity power factor operation at PCC and stabilizes the DC-link voltage at 900 V (± 5%), ensuring reliable operation.

Keywords Harmonic mitigation, Indirect current control strategy, Maximum power point tracking, PV-DSTATCOM, Power quality, Reactive power compensation, Real-time simulation, Total harmonic distortion (THD)

The rising integration of photovoltaic (PV) systems into power distribution networks presents significant challenges in maintaining grid stability and power quality[1]. While PV energy is a sustainable solution, its intermittent nature, combined with non-linear and unbalanced loads, causes harmonic distortions, reactive power imbalances, and voltage fluctuations at the point of common coupling (PCC)[1–4]. These issues contribute to increased power losses, equipment malfunctions, and potential non-compliance with regulatory standards[5,6]. In three-phase four-wire power distribution networks, unbalanced loading and harmonic currents further intensify these challenges, causing excessive heating of neutral conductor[7–11]. Effective mitigation strategies are a requisite to ensure reliable grid operation. A PV-based distribution static compensator (PV-DSTATCOM) presents a promising solution by facilitating seamless PV integration while enhancing power quality[12]. However, real-time performance of PV-DSTATCOM under practical grid conditions requires thorough evaluation. Factors such as balanced and unbalanced PCC voltages, fluctuating solar irradiance level, and sudden non-linear load variations can significantly impact its effectiveness[13].

Background research

The integration of PV systems into power distribution networks has led to extensive research on power quality improvement techniques. A variety of solutions, such as distribution static compensators (DSTATCOMs), active power filters (APFs), and other custom power devices, have been widely investigated to mitigate issues like harmonic distortions, reactive power imbalances, and voltage fluctuations at the PCC[14–16]. Among these, voltage-source converter (VSC)-based DSTATCOMs have gained significant attention due to their ability to provide dynamic compensation under varying grid/PCC voltage conditions[17–21]. Table 1 presents an overview of PV grid-integrated systems, summarizing the key focus areas, and key findings of various studies.

[1]Dr. A.P.J. Abdul Kalam Technical University, Lucknow, India. [2]Department of Electrical Engineering, Power and Energy Research Centre, Kamla Nehru Institute of Technology, Sultanpur, India. [3]Department of Electrical Engineering, Institute of Engineering and Technology, Lucknow, India. ✉email: vinamragovil1985@gmail.com

References	Year	Key focus	Key Findings
[2]	2021	DC-link voltage control under conditions of capacitance degradation, with the application of a Secondary Control Strategy	Ensured stable voltage regulation despite capacitor aging, enhancing system reliability
[4]	2022	Voltage stability in AC-DC microgrids, utilizing Fuzzy-Based Controllers and Interval Type-II Fuzzy Logic	Enhanced voltage stability and improved power quality in AC-DC microgrids
[7]	2022	PV grid interfaced system, utilizing Space Vector Modulation (SVM) and Selective Harmonic Elimination (SHE)	Optimized system performance, improving voltage profile and reducing THD
[8]	2021	Reduced switch multilevel inverter for DSTATCOM, using a Cascaded H-bridge Multilevel Inverter	Simplified architecture while achieving effective power quality enhancement
[11]	2022	The study examines power quality in EV charging stations, using Voltage-Oriented Control (VOC) and Current-Oriented Control (COC)	Stabilized voltage and minimized harmonic distortion, improving power quality at EV stations
[16]	2022	PV and hybrid energy systems, employing Intelligent Tuning and a Fuzzy-Based DSTATCOM	Enhanced dynamic response and better power compensation during fluctuations
[18]	2022	Weak grid-connected wind energy systems, utilizing FLSRF Controlled D-STATCOM	Improved grid performance and resilience to voltage fluctuations in weak grid conditions
[22]	2022	Real-time power quality enhancement through Neural Network-Based Intelligent Control	Improved adaptability to dynamic grid changes, enhancing system response
[23]	2024	Simulation of grid-connected DSTATCOM, applying PWM Voltage Control and Hysteresis Current Control	Demonstrated the importance of accurate control algorithms for maintaining optimal power quality in grid systems
[24]	2023	Grid-tied PV systems utilizing Hysteresis and PI Controllers	PI controller ensured better stability, while Hysteresis provided superior dynamic response
[25]	2021	Grid-tied SPV-DSTATCOM under dynamic load conditions	Reduced THD and demonstrated good response to varying load conditions
[26]	2020	Active current control in a grid-tied PV system, accounting for variations in solar insolation during both day and night	Enhanced power quality by utilizing available inverter capacity to adapt to solar variations throughout the day
[27]	2025	Comparative analysis of FLC and PI controllers in a Malaysian microgrid for optimizing battery SOC and minimizing THD	FLC improved adaptability to renewables, while PI effectively minimized THD, enhancing grid stability
[28]	2024	ANN-based PI controller with virtual impedance for microgrid voltage control	AI-driven tuning enhanced THD reduction, power sharing, and system stability
[29]	2021	DSTATCOM in power distribution systems, employing Fractional Order Sliding Mode Control	Improved voltage regulation and power quality mitigation compared to conventional methods
This paper		Real-time simulation of PV-DSTATCOM using Typhoon HIL 604 for power quality enhancement under balanced and unbalanced PCC voltage conditions	Achieved effective THD reduction and optimized power extraction for enhanced power quality and reliable grid integration

Table 1. Overview of PV grid integration systems: key focus areas and findings.

The effectiveness of a DSTATCOM depends largely on the adopted control strategy, with direct and indirect current control methods being the two primary approaches[18,28]. In the direct current control strategy, both the load current and VSC current are sensed to determine the required compensating current. The controller actively forces the VSC to inject this compensating current so that the grid/source current remains sinusoidal and balanced. This method provides a fast dynamic response but has certain drawbacks, including variable switching frequency, increased power losses, and higher stress on power electronic switches[9,30,31]. Additionally, maintaining DC-link voltage stability under unbalanced and nonlinear load conditions can be challenging[22,32,33]. Conversely, the indirect current control strategy relies only on source/grid current sensing, eliminating the need for load and VSC current measurement. Instead of directly controlling the output current, the controller derives the required compensating reference indirectly by processing the grid current data. This approach improves DC-link voltage stability[23,34], reduces THD, minimizes switching losses, and ensures effective compensation of power quality disturbances. Its computational efficiency and robust performance under dynamic load variations make it particularly well-suited for PV-DSTATCOM applications[35,36].

Parallel to these developments, extensive research has been reported on grid-connected PV systems, with a strong focus on maximum power point tracking (MPPT), power injection, and grid synchronization[40,41]. While conventional PV systems using VSCs primarily focus on active power injection, recent advancements in PV-DSTATCOM technology enable VSCs to concurrently inject active power and enhance power quality through reactive power compensation and harmonic mitigation[23,24]. Unlike traditional systems, PV-DSTATCOMs can compensate for reactive power, mitigate harmonics, and stabilize PCC voltage, offering enhanced grid support beyond simple power generation[25,37,38,42].

Several studies have explored PV-DSTATCOM operation under various grid conditions, demonstrating effective harmonic mitigation, reactive power compensation, and DC-link voltage regulation[26]. However, many existing studies are limited to steady-state analysis or simplified simulation models, with less emphasis on comprehensive real-time validation under practical conditions[24,27,28]. Various control strategies and MPPT methods for PV grid integration, along with their reported THD values and key findings, are summarized in Table 2.

Research gaps, objectives and contributions

Despite notable advancements in PV-DSTATCOM technology, much of the existing research remains focused on steady-state analysis and offline simulations, providing limited insights into real-time performance under practical grid conditions. Unbalanced PCC voltages, fluctuating solar irradiance, and sudden nonlinear load variations etc. present challenges that require further exploration in existing studies. While various harmonic

References	Year	Control strategy	Voltage condition	THD reported	Key findings
[20]	2023	Hybrid active power filter (HAPF) vs. distribution static compensator (D-STATCOM) and P&O-MPPT	Balanced grid voltage	5.71% (DSTATCOM) 1.91% (HAPF)	HAPF outperformed D-STATCOM in THD reduction
[23]	2024	Hysteresis current control vs. sinusoidal PWM (SPWM) control	Balanced grid voltage	4.56%	SPWM generally outperformed Hysteresis control, but an optimized hysteresis band improved its effectiveness in specific cases
[37]	2023	Adaptive THD control based on irradiance levels and P&O-MPPT	Balanced grid voltage	5.50%	Mitigated THD fluctuations with changing irradiance, improving stability
[38]	2022	Hysteresis with dynamic fixed carrier exchange algorithm (DFCEA) & INC-MPPT	Balanced grid voltage	< 5.00%	Consistent switching and significant THD reduction
[27]	2025	Indirect current control (ICC) + ANN-based adaptive control & ANN-MPPT	Balanced grid voltage	3.20%	Optimized performance under variable loads with significant THD reduction
[28]	2024	ANN-PID hybrid controller and perturb & observe with ANN optimization	Balanced grid voltage	3.36%	AI-based tuning enhanced THD reduction and system stability
[14]	2024	Current Limiting control strategy	Unbalanced grid voltage	< 5%	Ensured stable operation under both normal and faulted grid conditions using a stationary reference frame
[39]	2024	VSS-LMS adaptive filter-based PLL-less scheme	Unbalanced grid voltage	5.62%	Demonstrated faster convergence and robust harmonic rejection, improving power quality in practical grid scenarios
This paper		Indirect current control strategy + P&O MPPT	Balanced and unbalanced PCC/grid voltage	3.03–5.58% (Balanced PCC voltage); 3.95–5.93% (Unbalanced PCC voltage)	Achieved effective THD reduction across varying PCC voltages, enhancing power quality

Table 2. Control strategies for PV grid integration: summary of reported THD and key findings.

mitigation strategies have been explored, further investigation is needed to comprehensively assess their ability to ensure consistent compliance with IEEE-519 standards across diverse operating scenarios. Addressing these research gaps is crucial for enhancing the reliability and effectiveness of the PV-DSTATCOM systems in power distribution networks.

This paper formulates following research objectives to bridge these research gaps:

- Investigating the dynamic transition between pure DSTATCOM mode (operating during night-time or when PV generation is unavailable) and PV-DSTATCOM mode, where the system simultaneously performs harmonic mitigation, reactive power compensation, and active power injection under varying solar irradiance conditions.
- Evaluating the impact of grid/PCC voltage unbalance on the effectiveness of harmonic suppression, reactive power compensation, and neutral current regulation in a three-phase four-wire power distribution network.
- Analyzing the real-time response of PV-DSTATCOM to sudden nonlinear load variations and its ability to maintain power quality under both balanced and unbalanced PCC voltage conditions.
- Assessing the ability of the system to maintain a stable DC-link voltage and balanced source/grid currents under varying solar irradiance levels, sudden non-linear load variations, and varying grid/PCC voltage conditions.
- Conducting a comprehensive assessment of the effectiveness of the system in achieving consistent compliance with IEEE-519 harmonic standards across different operating scenarios, including variations in solar irradiance, sudden non-linear load variations, and varying grid/PCC voltage conditions.

To address the identified research gaps, this paper makes the following contributions:

- Development of a high-fidelity real-time simulation model of PV-DSTATCOM system using Typhoon HIL 604, enabling precise evaluation of system performance under practical grid conditions, including both balanced and unbalanced PCC voltages.
- Implementation of an indirect current control strategy that requires only source/grid current sensing, eliminating the need for load and/or VSC current measurements. This improves control efficiency while ensuring precise neutral current regulation and stable DC-link voltage.
- Comprehensive real-time validation of PV-DSTATCOM system operation, demonstrating its ability to seamlessly transition between pure DSTATCOM mode (for reactive power support and harmonic mitigation) and PV-DSTATCOM mode (for simultaneous active power injection and power quality enhancement) under dynamic solar irradiance conditions.
- Evaluation of the harmonic suppression under IEEE-519 standards, by analyzing the system's ability to mitigate harmonics and maintain power quality under fluctuating load and grid conditions in a three-phase four-wire power distribution network.

Organisation of the paper

This paper is structured as follows: Section "Introduction" provides the background, research gap, objectives, and contributions. Section "System configuration" outlines the system configuration, component sizing, and parameter selection for the proposed PV-DSTATCOM. Section "Indirect current control strategy" details the

indirect current control strategy. Section "Real-time simulation, results and discussions" presents real-time simulations evaluating PV-DSTATCOM performance under varying solar irradiance and load fluctuations, considering both balanced and unbalanced PCC voltages. Finally, Section "Conclusion" summarizes the conclusions and suggests directions for future research.

System configuration

The proposed PV-DSTATCOM system, as illustrated in Fig. 1, consists of a PV array, a boost converter, a split-capacitor DC link, and a two-level VSC. The VSC enables efficient PV power injection while dynamically regulating the reactive power to enhance power quality at the PCC. The MPPT algorithm optimally adjusts the duty cycle of the boost converter to ensure maximum power extraction from the PV array [38]. By actively regulating the DC-link voltage and suppressing harmonics, the VSC facilitates seamless power transfer and improves overall power quality.

PV array, MPPT, and boost converter

The proposed 3.5 kW PV array operates under varying solar irradiance, requiring a MPPT algorithm for maximum energy extraction. Using perturb & observe (P&O) method, the MPPT algorithm dynamically adjusts the duty cycle of the boost converter, stepping up the PV voltage to match the DC-link voltage. This ensures that the PV array operates at its maximum power point (MPP) under changing solar irradiance conditions [43].

The P&O-based MPPT controller perturbs the duty cycle, monitors the PV array power output, and adjusts it accordingly––if power increases, the duty cycle is incremented; if power decreases, it is decremented. This iterative process enables continuous tracking of the MPP, maximizing energy harvest. The boost converter efficiently steps up the PV voltage while maintaining optimal duty cycle control. To prevent instability, the MPPT algorithm is bounded by upper and lower duty cycle limits.

The real-time decision-making process of MPPT algorithm is illustrated in Fig. 2, demonstrating how the system adapts to fluctuating solar irradiance conditions, ensuring maximum power extraction. The detailed PV panel specifications and array sizing are provided in Table 3.

DC-link capacitor and PV power transfer

The split-capacitor DC link acts as an energy buffer between the PV system and the VSC while power transfer from the PV system to the PCC [34]. The DC-link voltage dynamics are governed by:

$$0.5C\frac{d}{dt}V_{DC} = \frac{P_{pv} - P_{VSC}}{V_{DC}} \tag{1}$$

where symbols are listed in Table 4.

VSC and voltage dynamics at the PCC

The 7 kVA VSC serves as a dual-interface, enabling PV power injection and DSTATCOM operations for harmonic mitigation and reactive power compensation. It regulates the DC-link voltage (V_{DC}) at its reference value by dynamically adjusting the active power transferred by the VSC (P_{VSC}) to the PCC, ensuring it matches the power extracted from the PV array (P_{pv}) and maintaining power balance. For reliable operation under worst-case conditions, the reference DC-link voltage (V_{DC}^*) must accommodate the highest peak voltage at the lowest modulation index. Considering a 415 V RMS (line-to-line) grid/PCC voltage and a typical sinusoidal PWM modulation index range of 0.85 to 1, the minimum required V_{DC}^* is calculated to be 797.19 V. Therefore, a value of $V_{DC}^* = 900$ V is selected in this paper to ensure proper operation.

Additionally, the VSC provides up to 6 kVAr of reactive power support to enhance power quality at the PCC. Operating under an indirect current control scheme [23,44], the VSC effectively mitigates harmonics, compensates reactive power, and improves the power factor, ensuring stable grid interaction. The voltage dynamics at the PCC are governed by:

$$e_{dg} - \nu_{dvsc} = L_g\left(\frac{d}{dt}i_{dg}\right) + R_g i_{dg} - \omega_g L_g i_{qg} \tag{2}$$

$$e_{qg} - \nu_{qvsc} = L_g\left(\frac{d}{dt}i_{qg}\right) + R_g I_{qg} + \omega_g L_g i_{dg} \tag{3}$$

where symbols are listed in Table 4.

Indirect current control strategy

The indirect current control strategy offers an efficient and robust method for regulating the VSC in a PV-DSTATCOM system (see Fig. 1), ensuring precise PV power injection and enhanced power quality at the PCC [24]. Unlike direct current control, which derives reference currents from load currents and directly regulates VSC currents, the indirect approach calculates reference currents based on source/grid currents [21,25]. This method is termed "indirect" because it does not require direct measurement of VSC or load currents; rather, it controls the VSC using source/grid current behavior. By eliminating direct current sensing, the strategy simplifies system implementation, reduces hardware complexity, and enhances reliability under varying PV generation and nonlinear load conditions. Its primary goals are to regulate the DC-link voltage for efficient PV power transfer, mitigate harmonics, and compensate for reactive power to improve overall grid power quality [23].
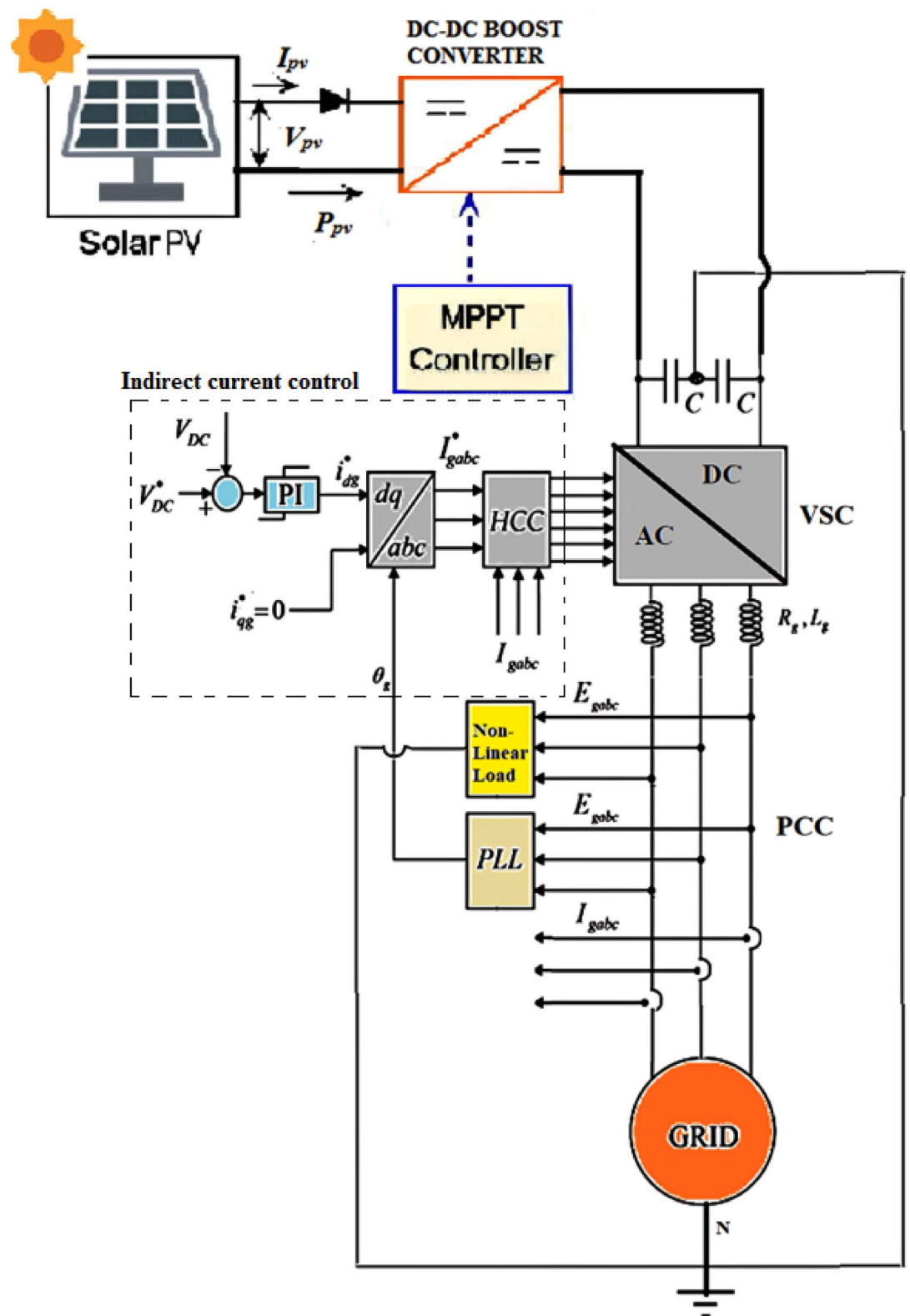
Fig. 1. Schematic of PV-DSTATCOM system utilizing an indirect current control scheme for power quality enhancement.
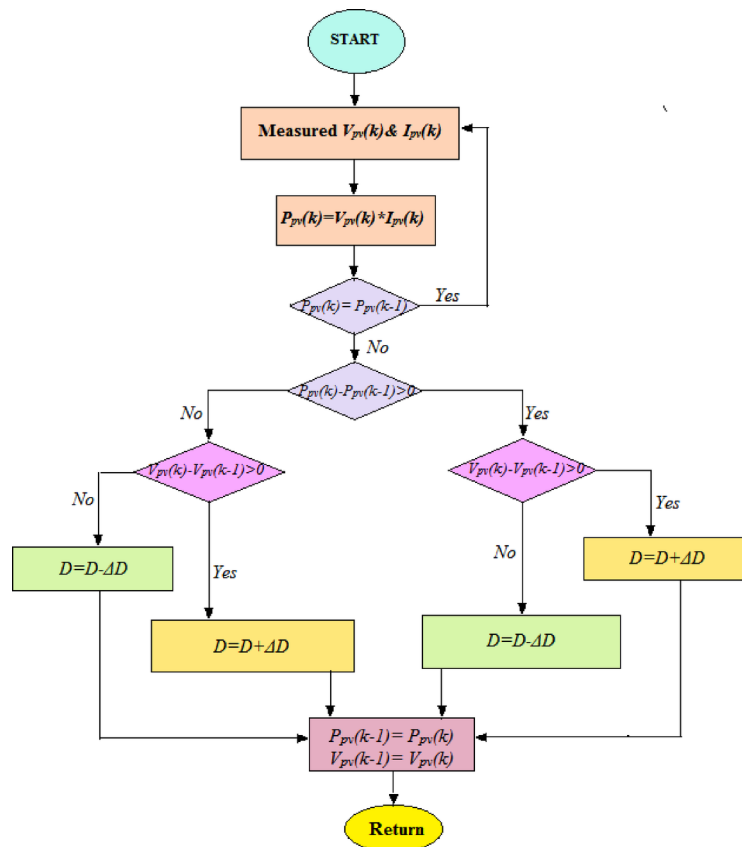
Fig. 2. Flowchart of the P&O algorithm for MPPT.

The control system consists of two key loops––an outer voltage control loop with a proportional-integral (PI) controller and an inner current control loop based on hysteresis. The outer loop stabilizes the DC-link voltage by balancing power exchange between the PV system and the grid. The error between the reference DC-link voltage (V_{DC}^*) and the actual DC-link voltage (V_{DC}) is processed by the PI controller to generate the reference d-axis source/grid current $\left(i_{dg}^*\right)$[44] as follows:

$$i_{dg}^* = \left(K_{pv} + \frac{K_{iv}}{s} \right) \cdot (V_{DC}^* - V_{DC}) \tag{4}$$

where symbols are listed in Table 4.

The calculations for PI controller gains (K_{pv} and K_{iv}) are systematically presented in Table 3. These gains have been derived using the symmetric optimum approach for PI tuning, a well-established method ensuring a balance between dynamic response and system stability. The detailed explanation of this approach is provided in[44,45].

By adjusting i_{dg}^*, the VSC ensures stable DC-link voltage despite fluctuations in solar irradiance and load demand, ensuring continuous PV power transfer to the PCC. To achieve unity power factor (UPF) at the PCC, the reference q-axis source/grid current (i_{qg}^*) is set to zero, ensuring the VSC manages all reactive power compensation. The inner current control loop processes the error between the reference and actual three-phase grid currents using a hysteresis current controller, which generates the switching signals for the VSC. This ensures sinusoidal grid currents, effective harmonic mitigation, and reactive power compensation. By injecting compensating currents, the VSC preserves grid voltage quality, reduces THD, and prevents nonlinear loads from degrading system performance.

Real-time simulation, results and discussions

To comprehensively evaluate the performance of the proposed PV-DSTATCOM system, real-time simulations are conducted using the Typhoon HIL 604 simulator, as shown in Fig. 3. The system parameters, detailed in Table 3 are carefully selected to represent practical operational conditions.

A key aspect of the performance assessment is the evaluation of the MPPT capability of PV array under varying irradiance conditions. Figure 4 illustrates the dynamic response of the PV array to solar irradiance levels of 0 W/m², 600 W/m², 1000 W/m², and 500 W/m², showcasing the effectiveness of the MPPT algorithm in maximizing power extraction. At nonzero irradiance levels, the PV array voltage remains stable, while the current and power output adjust accordingly, with recorded power outputs of 2080 W, 3440 W, and 1750 W,

Sr.	Parameter	Expression	Calculated value	Selected value	Refs.
PV panel					
1	Max. power (P_{mpp})	–	–	250W	–
2	Open circuit voltage of PV panel(V_{oc})	–	–	37.6 V	–
3	Short circuit current (I_{sc}) of PV panel	–	–	8.79 A	–
PV array					
4	Rated PVPower (P)	–	–	3.5 kW	[24]
5	Number of Panels (N_m)	$N_m = \frac{P}{Pmpp}$	$N_m = \frac{3500}{250} = 14$	14	[24]
6	Panels in series (N_s)	–	–	7	–
7	Panels in parallel (N_p)	–	–	2	–
8	PV array voltage output (V_{pv})	$V_{pv} = 0.8 \times V_{OC} \times N_S$	$V_{pv} = 0.8 \times 37.6 \times 7 = 210.56$ V	210.56 V	[24]
9	PV array current output (I_{pv})	$I_{pv} = 0.9 \times I_{SC} \times N_P$	$I_{pv} = 0.9 \times 8.79 \times 2 = 15.82$ A	15.82 A	[24]
Grid					
10	Grid voltage (V_{LL})	–	–	415 V	–
11	Grid frequency (f)	–	–	50 Hz	–
DC link voltage					
12	Reference DC link voltage (V_{DC}^*)	$V_{DC}^* > \frac{2\sqrt{2} \times V_{LL}}{\sqrt{3} \times m}$	$V_{DC}^* > \frac{2\sqrt{2} \times 415}{\sqrt{3} \times 0.85} = 797.19$ V	900 V	[33]
DC to DC boost converter					
13	Boost inductor	$L_b = \frac{V_{pv} \times (V_{DC} - V_{pv})}{f_{sw} \times 0.1 \times I_{pv} \times V_{DC}}$	$L_b = \frac{210.56 \times (900 - 210.56)}{10000 \times 0.1 \times 15.82 \times 900}$ $= 10.2$ mH	10 mH	[24]
14	Input capacitance	$C_{in} = \frac{I_{pv} \times (V_{DC} - V_{pv})}{f_{sw} \times 0.02 \times V_{pv} \times V_{DC}}$	$C_{in} = \frac{15.82 \times (900 - 210.56)}{10000 \times 0.02 \times 210.56 \times 900}$ $= 287.78 \, \mu F$	300 μF	[24]
VSC (PV-DSTATCOM)					
15	Rated VSC capacity (S_{VSC})	–		7.0 kVA	–
16	Capacity for Reactive power support (Q_{VSC})	$Q_{VSC} = \sqrt{S_{VSC}^2 - P^2}$	$Q_{VSC} = \sqrt{7.0^2 - 3.5^2} = 6.02$ kVAr	6.0 kVAr	–
17	Peak VSC current	$I_p = \frac{\sqrt{2} \times S_{VSC}}{\sqrt{3} \times V_{LL}}$	$I_p = \frac{\sqrt{2} \times 7000}{\sqrt{3} \times 415} = 13.77$ A	13.77A	[9]
18	Capacitance in the DC link configuration (C)	$C = \frac{0.9 \times I_p}{2\sqrt{2} \times \pi \times f \times 0.02 \times V_{DC}}$	$C = \frac{0.9 \times 13.77}{2\sqrt{2} \times 3.14 \times 50 \times 0.02 \times 900}$ $= 1550 \, \mu F$	1600 μF	[33]
19	Coupling inductance (L_g)	$L_g = \frac{\sqrt{3} \times m \times V_{DC}}{12 \times \alpha \times f_{sw} \times 0.02 \times I_p}$	$L_g = \frac{\sqrt{3} \times 0.85 \times 900}{12 \times 1.2 \times 10000 \times 0.02 \times 13.77}$ $= 33.4$ mH	34 mH	[9]
Symmetric optimum tuning of PI controller gains					
20	Sampling time for outer control loop (T_v)	–	–	700 μs	–
21	Proportional Gain (K_{pv})	$K_{pv} = \frac{2 \times C \times V_{DC}}{3 \times a \times e_{dg} \times T_v}$	$K_{pv} = \frac{2 \times 1600 \times 10^{-6} \times 900}{3 \times 2.4142 \times 338.84 \times 700 \times 10^{-6}}$ $= 1.6765$	1.6765	[45]
22	Integral Gain (K_{iv})	$K_{iv} = \frac{K_p}{a^2 \times T_v}$	$K_{iv} = \frac{1.6765}{2.4142 \times 2.4142 \times 700 \times 10^{-6}}$ $= 410.92$	410.92	[45]

Table 3. Sizing and selection of system components and parameters for the proposed PV-DSTATCOM system.

respectively. Under zero irradiance (0 W/m²), the PV array voltage decreases significantly, leading to no power generation. The MPPT algorithm continually tracks the optimal operating point, ensuring maximum power extraction despite variations in irradiance. Furthermore, the simulation framework replicates a three-phase, four-wire distribution network, where the PV-DSTATCOM system employs a VSC with an indirect current control strategy. The VSC operates in two distinct modes to manage both active power injection and reactive power compensation:

- Pure DSTATCOM Mode (under no PV generation): The VSC prioritizes reactive power compensation and harmonic mitigation without injecting active power into the grid.
- PV-DSTATCOM Mode (under PV generation): The VSC injects active power into the grid while concurrently providing reactive power support and harmonic filtering.

To comprehensively assess system performance, three critical test cases are analyzed under both balanced and unbalanced PCC voltage conditions. These test cases evaluate the response of PV-DSTATCOM to variations

List of symbols			
a	Trade-off parameter (set to 2.4142) between damping and dynamic response in symmetric optimum-tuned pi control	L_g	Coupling inductance
C	Capacitance of each individual capacitor in the split-capacitor DC link configuration	m	Modulation index
C_{in}	Input capacitance of boost converter	N_m	Number of PV panels
D	Duty cycle of a boost converter in MPPT	N_p	Number of PV panels in parallel
ΔD	Change in duty cycle	N_s	Number of PV panels in series
E_{gabc}	Three-phase PCC/grid voltages	P_{mpp}	Rated maximum power of PV panel
e_{dg}	d-axis PCC/grid voltage	P	Rated power of PV array
e_{qg}	q-axis PCC/grid voltage	P_{VSC}	Active power injected by VSC to the grid
f	Grid frequency	Q_{VSC}	Capacity of VSC for reactive power support
f_{sw}	Converter switching frequency	R_g	Coupling Resistor
i_{dg}^*	Reference d-axis source/grid current	S_{VSC}	Rated VSC capacity
i_{dg}	d-axis source/grid current	T_v	Sampling time for outer control loop
I_{gabc}^*	Reference values of three-phase source/grid currents	V_{DC}	DC-link voltage
I_{gabc}	Three-phase grid/source currents	V_{DC}^*	Reference DC-link voltage
i_{qg}	q-axis source/grid Current	ν_{dvsc}	d-axis VSC voltage
i_{qg}^*	Reference q-axis source/grid Current	ν_{qvsc}	q-axis VSC voltage
I_p	Peak VSC current	V_{LL}	Line-to-line PCC/grid RMS voltage
I_{pv}	PV array current output	V_{oc}	Open circuit voltage of PV panel
I_{sc}	Short-circuit current of PV panel	V_{pv}	PV array voltage output
K_{iv}	Integral-gain of outer loop PI controller	ω_g	Angular grid frequency
K_{pv}	Proportional-gain of outer loop PI controller	θ_g	Grid phase angle
L_b	Boost inductance	α	Safety factor (set to 1.2)
List of abbreviations			
AI	Artificial intelligence	PCC	Point of common coupling
ANN	Artificial neural network	PI	Proportional-integral
COC	Current-oriented Control	PID	Proportional-integral-derivative
DC	Direct current	PLL	Phase-locked-loop
DFCEA	Dynamic fixed carrier exchange algorithm	PV	Photovoltaic
FLC	Fuzzy logic controller	PVD-STATCOM	Photovoltaic-based distribution static synchronous compensators
FLSRF	Fuzzy logic synchronous reference frame	PWM	Pulse width modulation
HAPF	Hybrid active power filter	SOC	State of charge
HCC	Hysteresis current controller	SPV-DSTATCOM	Solar photovoltaic based distribution static compensator
HIL	Hardware-in-the-loop	SVC	Static VAR compensator
ICC	Indirect current control	SVM	Space vector modulation
IEEE	Institute of electrical and electronics engineers	THD	Total harmonic distortion
kVA	Kilo-volt ampere	UPF	Unity power factor
kW	Kilo-watt	VAr	Volt-ampere reactive
LMS	Least mean square	VOC	Voltage-oriented control
MPP	Maximum power point	VSC	Voltage source converter
MPPT	Maximum power point tracking	VSS	Variable step-size
P&O	Perturb and observe		

Table 4. List of symbols and abbreviations.

in solar irradiance and sudden load changes, offering key insights into its adaptability under dynamic grid conditions. Additionally, each scenario examines the system's effectiveness in enhancing power quality and ensuring compliance with IEEE standards (see Table 5).

Case 1: performance under varying solar irradiance with fixed nonlinear load
This case evaluates the operational performance of the PV-DSTATCOM system as the solar irradiance varies from 0 W/m² (night-time, no solar power generation) to 600 W/m² (moderate solar generation), while maintaining a fixed nonlinear load at the PCC. The objective is to assess the system's ability to seamlessly transition between pure DSTATCOM mode (at zero irradiance) and PV-DSTATCOM mode (under PV generation), ensuring effective harmonic suppression, reactive power compensation, and DC link voltage regulation while injecting active

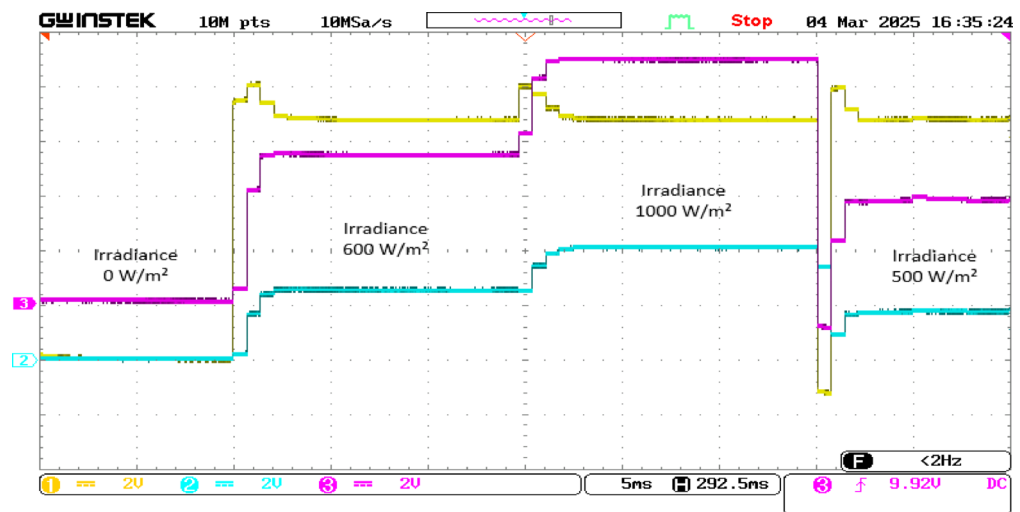**Fig. 3**. Typhoon HIL 604 simulator used for real-time simulation of the PV-DSTATCOM system.

Fig. 4. Dynamic response of the PV array for MPPT under varying solar irradiance levels. CH1: PV array voltage (100 V/div), CH2: PV array current (4A/div), CH3: PV array power (800W/div).

power into the grid. The real-time waveforms of three-phase PCC voltages and load currents for both balanced and unbalanced PCC voltage conditions are presented in Fig. 5, demonstrating the system's performance under these scenarios. The nonlinear load introduces harmonic distortions, with THD of load current measured at 13.51% under balanced PCC voltage, as depicted in Fig. 6a. Under unbalanced PCC voltage, the load current THD is slightly higher at 13.63%, as shown in Fig. 6b, due to asymmetry in supply voltages affecting harmonic propagation.

Balanced PCC voltage condition
Under balanced PCC voltage condition, a steady voltage profile can be seen at the PCC despite the nonlinear nature of the load. The real-time system response under different irradiance levels (0–600 W/m^2) is illustrated in Fig. 7a, c, and e for phases 'a,' 'b,' and 'c,' respectively. These waveforms capture the transition from DSTATCOM operation (at 0 W/m^2) to PV power injection mode (at 600 W/m^2) while sustaining power quality. The source/grid current waveforms in Fig. 7a, c, and e confirm the absence of active power injection at 0 W/m^2, where the VSC functions solely as a DSTATCOM, compensating for reactive power demand and mitigating harmonics. At this stage, the source/grid current is maintaining unity power factor at the PCC.

As the irradiance increases to 600 W/m^2, the VSC transitions into a dual-mode operation, simultaneously injecting active power into the grid while continuing to provide reactive power compensation and harmonic mitigation. The phase shift in the source/grid currents observed in Fig. 7 signifies active power transfer. Thus, the VSC effectively operates as a multifunctional device, addressing both power quality improvement and PV power injection into the PCC. The neutral current dynamics under balanced PCC voltage conditions, depicted in Fig. 8a, reveal that the source/grid neutral current remains near zero, which signifies effective load balancing

Cases	PCC Voltage Status	Irradiance (W/m^2)	Load THD (%)	Source/Grid THD (%)	DC Link Voltage	Source/Grid Neutral Current	Remarks
Case-1	Balanced	0 Night-time	13.51	5.58	Stable within ± 5%	Near zero	No active power injected, harmonic mitigation achieved, THD slightly exceeds IEEE-519 limit
	Balanced	600	13.51	4.08	Stable within ± 5%	Near zero	Active power injected, harmonic suppression remains effective, THD within IEEE-519 limits
	Unbalanced	0 Night-time	13.63	5.93	Stable within ± 5%	Near zero	Higher THD due to unbalanced PCC voltage, but harmonic mitigation continues
	Unbalanced	600	13.63	3.95	Stable within ± 5%	Near zero	Active power injection improves harmonic suppression, THD well within IEEE-519 standards
Case-2	Balanced	1000	13.51	4.96	Stable within ± 5%	Near zero	Active power injected as irradiance increases, THD within IEEE-519 limits
	Unbalanced	1000	13.63	5.17	Stable within ± 5%	Near zero	Voltage unbalance causes slight THD increase, but overall power quality remains stable
Case-3	Balanced	700	Before: 13.51 After: 9.40	Before: 4.88 After: 3.03	Stable within ± 5%	Near zero	Sudden load increase reduces THD, harmonic mitigation continues, THD stays within IEEE-519 limits
	Unbalanced	700	Before: 13.63 After: 9.36	Before: 5.77 After: 4.65	Stable within ± 5%	Near zero	Load increase reduces THD, but higher THD compared to balanced case due to voltage imbalance

Table 5. Performance summary of PV-DSTATCOM under varying irradiance and PCC voltage condition.
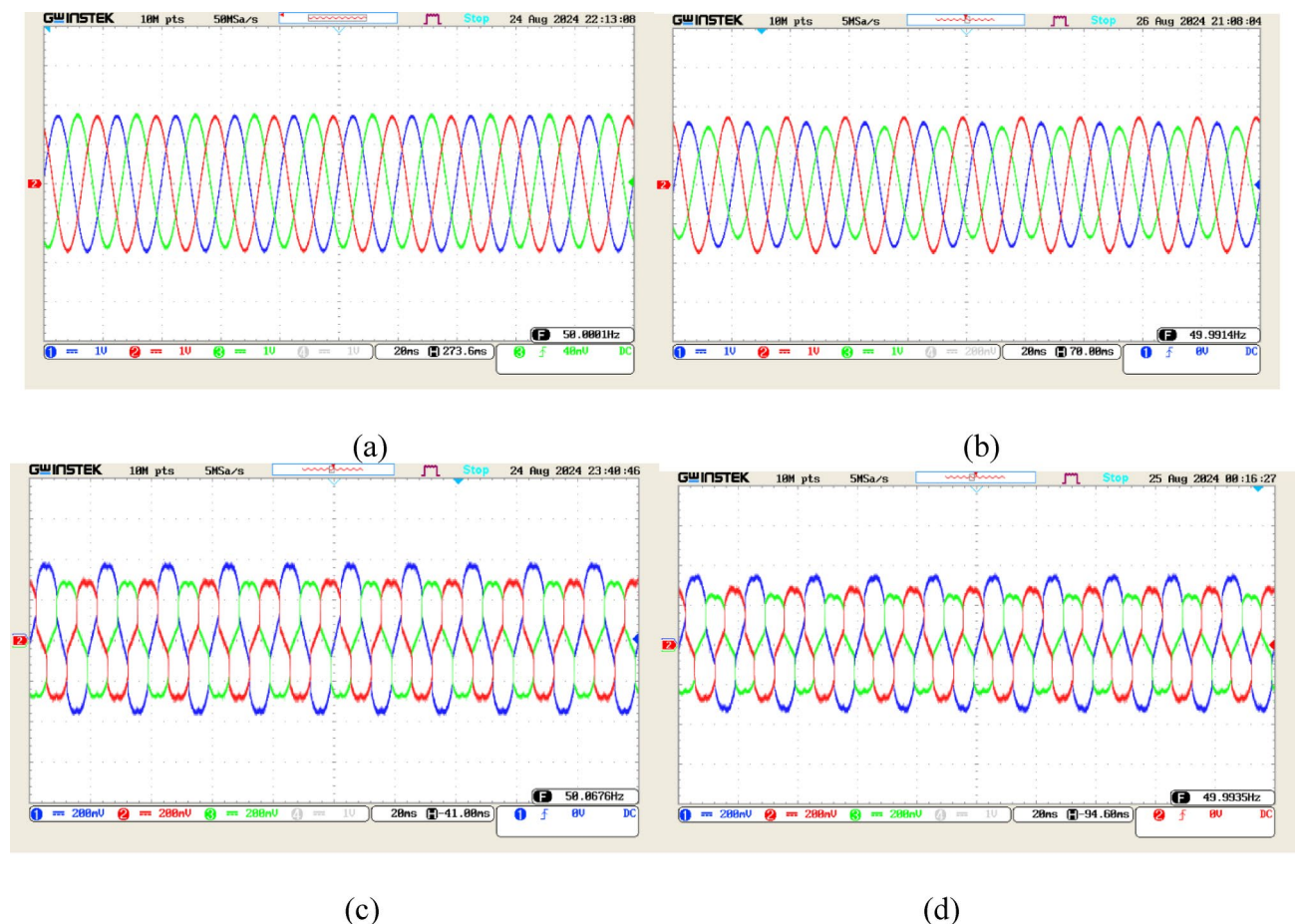

(a)

(b)

(c)

(d)

Fig. 5. Real-time waveforms of three-phase PCC voltages and load currents under a fixed non-linear load—(**a**) balanced PCC voltage waveforms (CH1 to CH3: 200 V/div), (**b**) unbalanced PCC voltage waveforms (CH1 to CH3: 200 V/div), (**c**) load current waveforms under balanced PCC voltage conditions (CH1 to CH3: 1A/div), and (**d**) load current waveforms under unbalanced PCC voltage conditions (CH1 to CH3: 1 A/div).
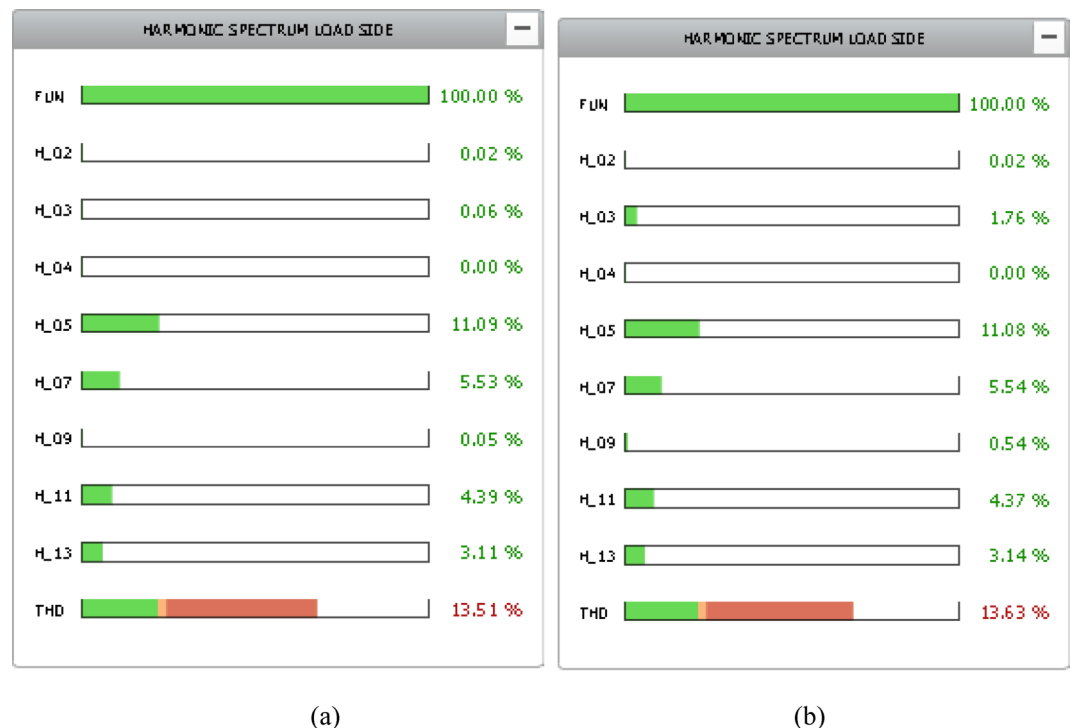
Fig. 6. Harmonic spectra of load current—(**a**) under balanced PCC voltage condition, and (**b**) under unbalanced PCC voltage condition.

and harmonic cancellation. However, nonzero neutral currents are observed in the VSC and load side, resulting from the inherent imbalance in nonlinear load current components. The DC-link voltage regulation is illustrated in Fig. 9a, where the DC-link voltage is maintained at approximately 900 V throughout the irradiance variations.

The grid current THD, which is a key indicator of power quality, remains within IEEE-519 harmonic standards at 600 W/m², recorded at 4.08%, as shown in Fig. 10c. However, at 0 W/m², where no active power injection occurs, the grid current THD slightly exceeds the IEEE-519 permissible limit, reaching 5.58%, as shown in Fig. 10a.

Unbalanced PCC voltage condition
Under unbalanced PCC voltage conditions, voltage asymmetry introduces additional distortions that can impact power quality. The real-time system response under different irradiance levels (0–600 W/m²) is illustrated in Fig. 7b, d, and f for phases 'a,' 'b,' and 'c', respectively. These waveforms capture the transition from pure DSTATCOM operation (at 0 W/m²) to PV power injection mode (at 600 W/m²), while maintaining power quality and reactive power compensation. Despite the presence of PCC voltage unbalance, the real-time waveforms in Fig. 7b, d, and f confirm that the source/grid currents remain nearly balanced, demonstrating the effectiveness of the PV-DSTATCOM in preventing excessive current distortions. The VSC continues to provide harmonic mitigation and reactive power support, ensuring that source/grid current waveforms do not exhibit severe phase imbalances or waveform asymmetries.

The neutral current behavior, as depicted in Fig. 8b, highlights the ability of the VSC to regulate the source/grid neutral current, ensuring it remains near zero despite the presence of unbalanced PCC voltage and nonlinear load. This indicates that the VSC effectively counteracts unbalanced load currents, maintaining load balancing and harmonic cancellation, even under non-ideal grid conditions. The DC-link voltage, as shown in Fig. 9b, remains stable at 900 V, reinforcing the robustness of the indirect control strategy.

At 0 W/m², when no active power injection occurs, the source/grid current THD slightly exceeds the IEEE-519 permissible limit, reaching 5.93%, as shown in Fig. 10b. This increase in distortion is attributed to the absence of active power support, which limits the ability of the VSC to improve the harmonic profile of the source/grid current. However, as the irradiance increases to 600 W/m², the PV-DSTATCOM injects active power, enhancing the harmonic suppression capability. Consequently, the source/grid current THD improves significantly and remains within IEEE-519 standards, recorded at 3.95%, as depicted in Fig. 10d.

This analysis confirms that even under unbalanced PCC voltage conditions, the PV-DSTATCOM effectively maintains power quality, regulates neutral current, and stabilizes the DC-link voltage, ensuring compliance with IEEE harmonic limits while mitigating the impact of voltage asymmetry on the PCC.

Case 2: performance under high solar irradiance condition with fixed non-linear load
This case evaluates the performance of the PV-DSTATCOM under high solar irradiance condition, ranging from 600 W/m² to 1000 W/m². This scenario is critical in assessing the system's capability to handle increased active
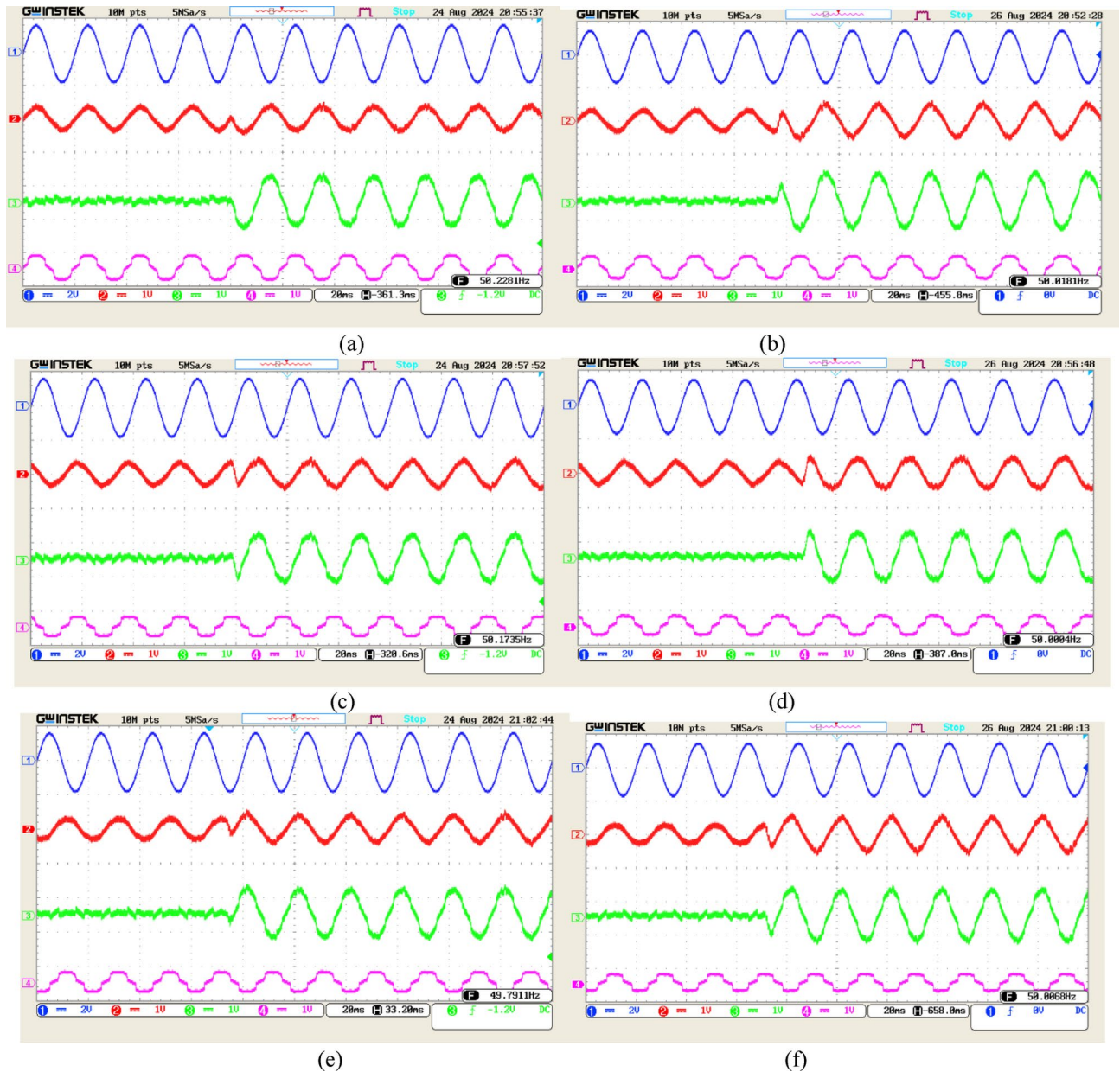
Fig. 7. Real-time performance waveforms of the proposed PV-DSTATCOM under a fixed non-linear load with varying irradiance levels (0–600 W/m²)—(**a**), (**c**), (**e**) performance waveforms under balanced PCC voltage condition for Phase 'a,' Phase 'b,' and Phase 'c,' respectively; (**b**), (**d**), (**f**) performance waveforms under unbalanced PCC voltage condition for Phase 'a,' Phase 'b,' and Phase 'c,' respectively.CH1: Phase 'a' PCC voltage (400 V/div); CH2: source/grid current waveform of respective phase (5A/div); CH3: VSC current waveform of respective phase (5A/div); CH4: load current waveform of respective phase (5A/div).

power injection into the grid while maintaining power quality, and harmonic mitigation. The system's response is examined under both balanced and unbalanced PCC voltage condition to ensure comprehensive performance validation.

Balanced PCC voltage condition
As depicted in Fig. 11a, c, and e, the load current remains constant due to its fixed nature, while increasing solar irradiance proportionally raises the VSC currents, consequently increasing the source/grid current. The neutral current regulation, illustrated in Fig. 12a, confirms that despite load imbalance, the source/grid-side neutral current remains near zero, demonstrating the system's strong load-balancing capability. This indicates that the VSC efficiently compensates for load asymmetry and minimizes neutral current disturbances at the PCC. Furthermore, Fig. 13a shows that the DC-link voltage remains stable at 900 V and source/grid currents remain balanced, with the THD of the grid current maintained at approximately 4.96%, well within IEEE-519
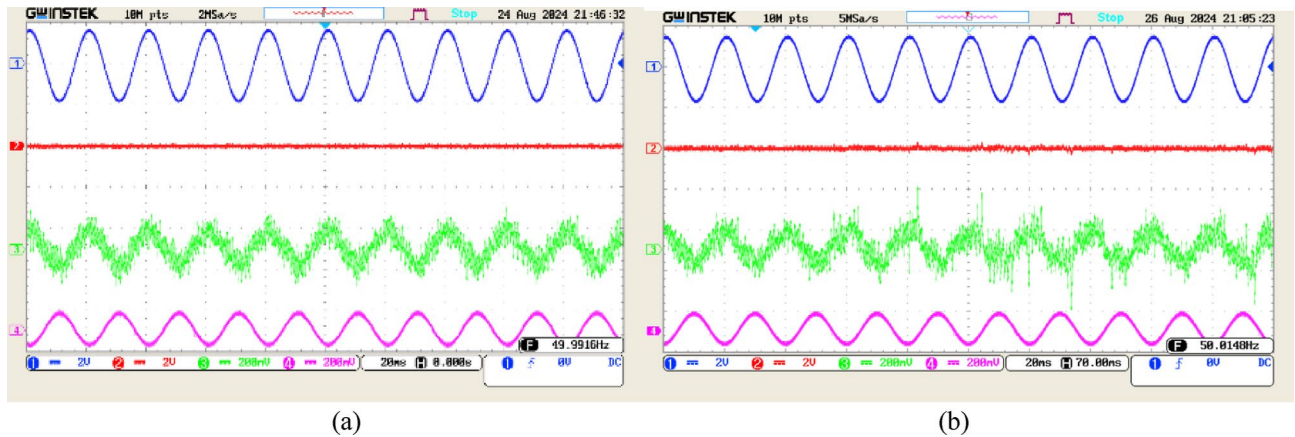
(a)   (b)

Fig. 8. Real-time waveforms of neutral currents under varying irradiance levels (0–600 W/m^2) with a fixed non-linear load—(**a**) neutral current waveforms under balanced PCC voltage condition; (**b**) neutral current waveforms under unbalanced PCC voltage condition. CH1: Phase 'a' PCC voltage (400 V/div); CH2: source/grid neutral current waveform (10A/div); CH3: VSC neutral current waveform (1A/div); CH4: load neutral current waveform (1A/div).

(a)   (b)
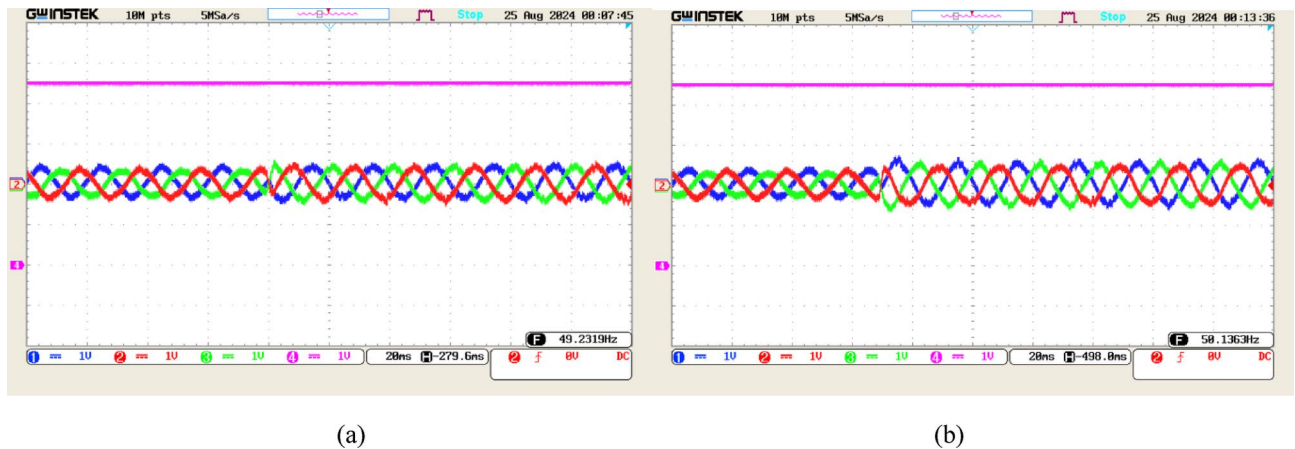
Fig. 9. Real-time waveforms of three-phase source/grid currents and DC-link voltage under varying irradiance levels (0–600 W/m^2) with a fixed non-linear load—(**a**) waveforms under balanced PCC voltage condition, and (**b**) waveforms under unbalanced PCC voltage condition. CH1 to CH3: source/grid current waveforms (5 A/div); CH4: DC-link voltage (200 V/div).

standards (see Fig. 14a). This result highlights the ability of the PV-DSTATCOM to ensure high power quality preventing excessive harmonic distortion while injecting maximum available PV power into the grid.

Unbalanced PCC voltage condition
When operating under unbalanced PCC voltage condition, the system exhibits similar trends to those observed in the balanced case, as shown in Fig. 11b, d, and f. The VSC and source/grid currents continue to increase in response to higher solar irradiance, confirming the system's ability to support active power transfer despite voltage unbalance. The neutral current behaviour, depicted in Fig. 12b, remains consistent with the balanced case, indicating that the grid-side neutral current is effectively suppressed, ensuring that load imbalances do not propagate to the grid.

Furthermore, Fig. 13b shows that the DC-link voltage remains stable at 900 V and source/grid currents remain balanced despite unbalanced PCC voltage. However, due to the voltage asymmetry at the PCC, the grid current THD slightly exceeds the IEEE-519 threshold, reaching 5.17%, as illustrated in Fig. 14b. This increase in distortion is attributed to the combined effects of nonlinear loads and PCC voltage unbalance. Despite this, the system maintains stable DC-link voltage and effective reactive power compensation, ensuring reliable operation under real-world grid condition.
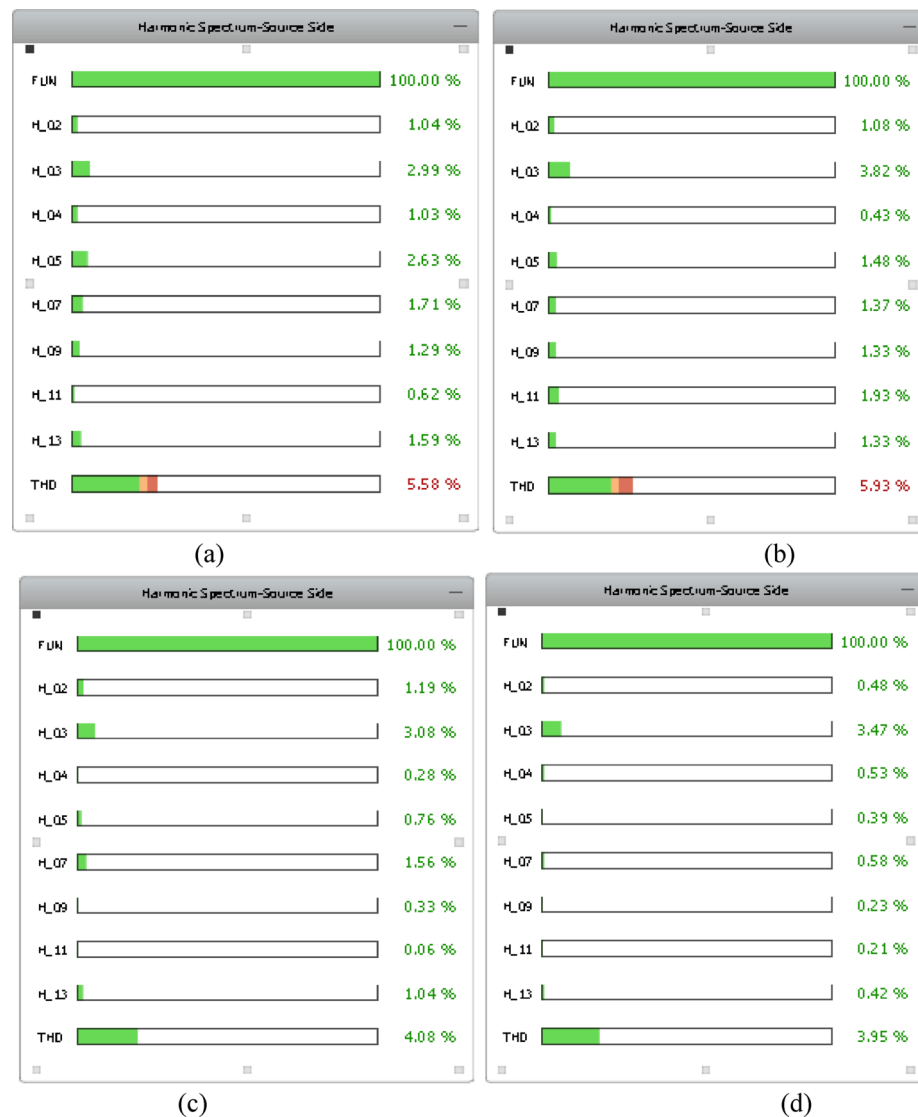
Fig. 10. Harmonic spectra of source/grid current under a fixed non-linear load—(**a**) under balanced PCC voltage condition with PV power injection at an irradiance level of 0 W/m², (**b**) under unbalanced PCC voltage condition with PV power injection at an irradiance level of 0 W/m², (**c**) under balanced PCC voltage condition with PV power injection at an irradiance level of 600 W/m², and (**d**) under unbalanced PCC voltage condition with PV power injection at an irradiance level of 600 W/m².

Case 3: impact of sudden non-linear load variations at fixed solar irradiance

This case investigates the transient response of PV-DSTATCOM to a sudden increase in nonlinear load while maintaining a fixed solar irradiance of 700 W/m². This test is crucial for assessing transient stability and power quality management under dynamic load condition. The performance of system is analyzed under both balanced and unbalanced PCC voltage condition.

Balanced PCC voltage condition
As depicted in Fig. 15a, the real-time waveforms of three-phase load currents demonstrate a sudden step increase in nonlinear load under balanced PCC voltage condition. This abrupt change leads to a shift in harmonic distortion levels, with the load current THD reducing from 13.51% to 9.40%, as shown in Fig. 16a and c. The THD reduction occurs because the increase in load results in a higher fundamental current component, thereby reducing the relative impact of harmonic distortions. Despite the sudden load variation, the VSC maintains stable compensation, effectively mitigating harmonics and regulating reactive power. This is validated by the source/grid phase currents illustrated in Fig. 17a, c, and e. Since PV generation remains constant, the source/grid current magnitude decreases due to the increased local load demand, as the system prioritizes supplying the local load before exporting excess power to the source/grid.

Figure 18a illustrates that the VSC effectively suppresses the source/grid-side neutral current, maintaining it close to zero despite nonlinear load imbalance and sudden load variations. Additionally, as shown in Fig. 19a, the
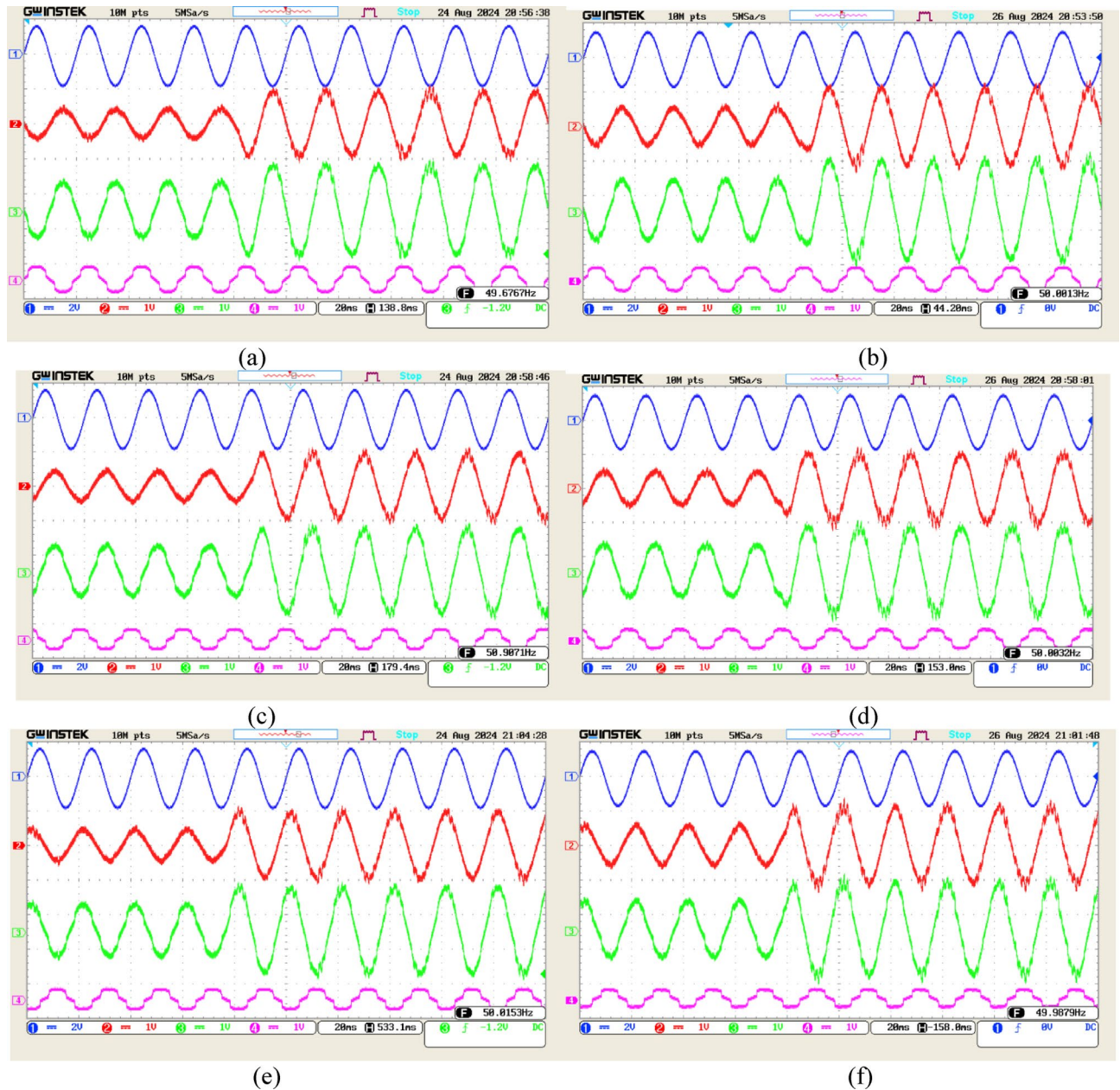
Fig. 11. Real-time performance waveforms of the proposed PV-DSTATCOM under a fixed non-linear load with varying irradiance levels (600–1000 W/m^2)—(**a**), (**c**), (**e**) performance waveforms under balanced PCC voltage condition for Phase 'a,' Phase 'b,' and Phase 'c,' respectively; (**b**), (**d**), (**f**) performance waveforms under unbalanced PCC voltage condition for Phase 'a,' Phase 'b,' and Phase 'c,' respectively. CH1: Phase 'a' PCC voltage (400 V/div); CH2: source/grid current waveform of respective phase (5A/div); CH3: VSC current waveform of respective phase (5A/div); CH4: load current waveform of respective phase (5A/div).

DC-link voltage remains stable at 900 V, demonstrating the robustness of the indirect current control strategy for the PV-DSTATCOM, even under sudden load change. Furthermore, the source/grid currents remain balanced, indicating the system's capability to mitigate load-induced distortions. The harmonic spectra of the source/grid current before and after the load change are presented in Fig. 20a and c, respectively. It is evident that the source/grid current THD remains within IEEE-519 permissible limits, confirming the effectiveness of PV-DSTATCOM in maintaining high power quality under rapid load disturbances.

Unbalanced PCC voltage condition
As depicted in Fig. 15b, the real-time waveforms of three-phase load currents exhibit a sudden step increase in nonlinear load under unbalanced PCC voltage condition. This transition leads to a reduction in load current THD from 13.63% to 9.36%, as illustrated in Fig. 16b and d, which follows the principle of increased fundamental current dominance. Despite the PCC voltage unbalance, the VSC effectively maintains compensation, ensuring
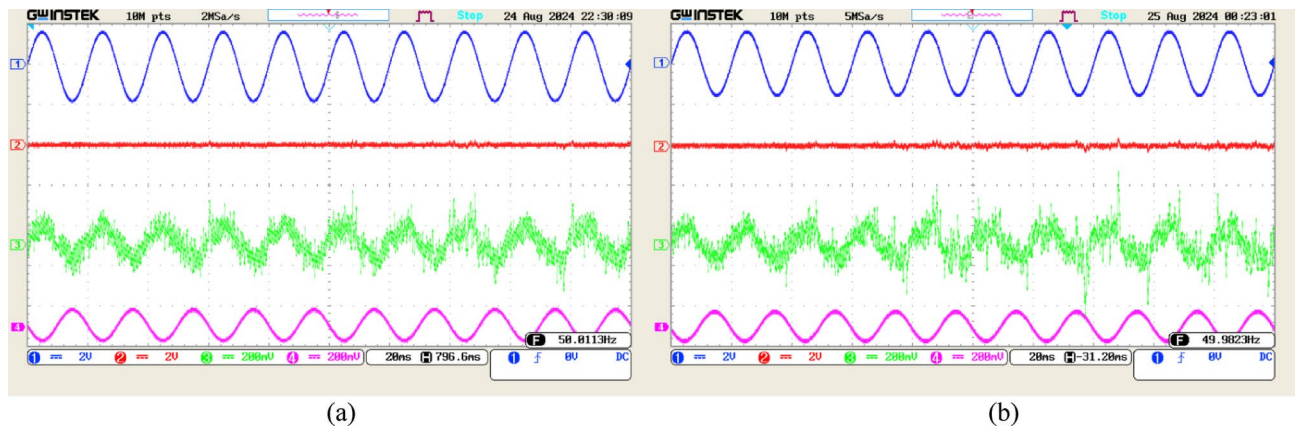

(a)   (b)

Fig. 12. Real-time waveforms of neutral currents under varying irradiance levels (600–1000 W/m^2) with a fixed non-linear load—(**a**) neutral current waveforms under balanced PCC voltage condition; (**b**) neutral current waveforms under unbalanced PCC voltage condition. CH1: Phase 'a' PCC voltage (400 V/div); CH2: source/grid neutral current waveform (10A/div); CH3: VSC neutral current waveform (1A/div); CH4: load neutral current waveform (1A/div).

(a)   (b)
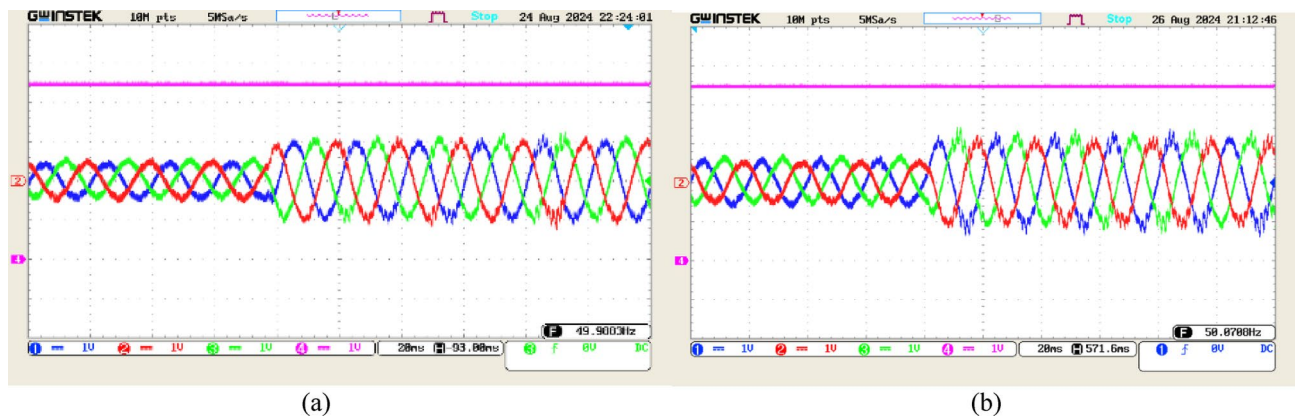
Fig. 13. Real-time waveforms of three-phase source/grid currents and DC-link voltage under varying irradiance levels (600–1000 W/m^2) with a fixed non-linear load—(**a**) waveforms under balanced PCC voltage condition, and (**b**) waveforms under unbalanced PCC voltage condition. CH1 to CH3: source/grid current waveforms (5 A/div); CH4: DC-link voltage (200 V/div).

stable source/grid phase currents, as shown in Fig. 17b, d, and f. Since the solar irradiance remains constant at 700 W/m^2, the increased local load demand results in a reduction in source/grid current magnitude. This behavior confirms the system's ability to dynamically adjust power allocation while maintaining grid support and power quality.

The neutral current dynamics, illustrated in Fig. 18b, indicate that the VSC efficiently suppresses the source/grid neutral current, maintaining it near zero despite the combined effects of nonlinear load imbalance and PCC voltage asymmetry. Additionally, the DC-link voltage remains stable at 900 V, as depicted in Fig. 19b, validating the robustness of the indirect current control strategy under unbalanced PCC voltage condition. Furthermore, the source/grid currents remain nearly balanced, highlighting the effectiveness of the VSC in mitigating the impacts of load unbalance, load disturbances, and PCC voltage asymmetry. The harmonic spectra of the source/grid current before and after the load change under unbalanced PCC voltage condition are presented in Fig. 20b and d, respectively. While the source/grid current THD remains within the acceptable IEEE-519 limits, it is slightly higher compared to the balanced PCC voltage scenario. This increase is primarily attributed to voltage asymmetry at the PCC, which induces additional harmonic distortions in the system.

Conclusion
This paper conducted a real-time evaluation of a PV-DSTATCOM system, demonstrating its effectiveness in MPPT, harmonic mitigation, reactive power compensation, and active power injection using the Typhoon HIL 604 simulator. The indirect current control strategy ensured precise DC-link voltage regulation at 900 V ($\pm 5\%$) and accurate reference current generation, enhancing system stability and reliability. The MPPT algorithm optimized power extraction, maintaining stable PV operation under varying irradiance levels. The PV array
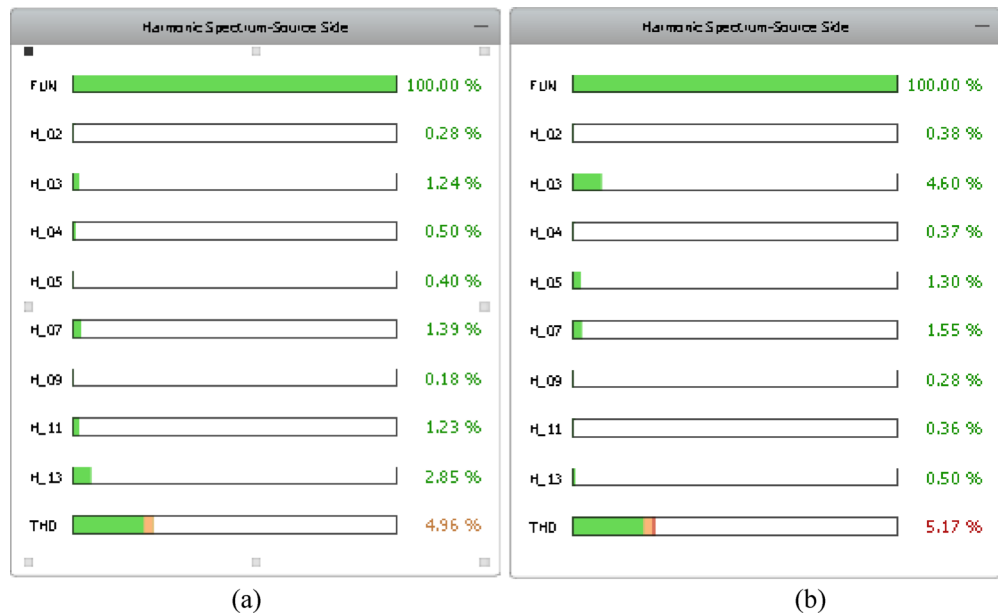
(a) (b)

Fig. 14. Harmonic spectra of source/grid current under a fixed non-linear load—(**a**) under balanced PCC voltage condition with PV power injection at an irradiance level of 1000 W/m², (**b**) under unbalanced PCC voltage condition with PV power injection at an irradiance level of 1000 W/m².
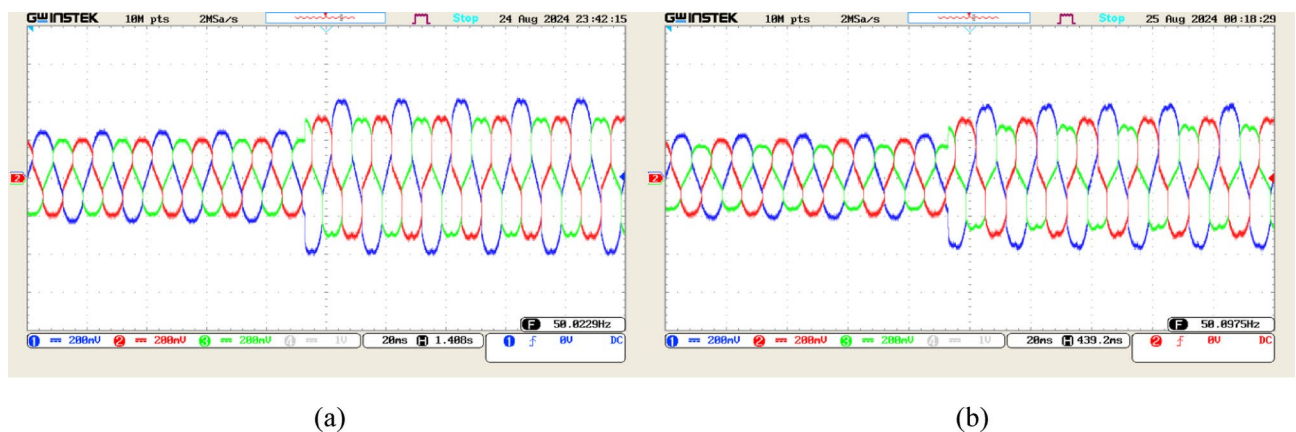

(a) (b)

Fig. 15. Real-time waveforms of three-phase load currents under a sudden load change—(**a**) load current waveforms under balanced PCC voltage condition, and (**b**) load current waveforms under unbalanced PCC voltage condition.CH1 to CH3: load current waveforms (1 A/div).

generated 2080 W, 3440 W, and 1750 W at 600 W/m2, 1000 W/m2, and 500 W/m2, respectively, with power dropping to zero at 0 W/m2. Continuous MPP tracking improved energy conversion efficiency, ensuring reliable PV-grid integration.

The PV-DSTATCOM significantly enhanced power quality, reducing THD to 3.03%–5.58% under balanced PCC voltage and 3.95%–5.93% under unbalanced conditions, adhering to IEEE-519 standards. Additionally, the proposed system maintained near-unity power factor operation at the PCC and effectively minimized source/grid neutral current, contributing to enhanced grid stability and reduced power losses. Seamless mode transitions were achieved, with DSTATCOM mode mitigating harmonics and compensating reactive power during night-time, while PV-DSTATCOM mode injected active power while maintaining power quality under high solar availability. Overall, the PV-DSTATCOM system demonstrated a robust and efficient solution for grid-integrated PV applications, ensuring stable and reliable power quality improvement.

Future research could explore adaptive control strategies to further enhance harmonic suppression, reactive power compensation, and system resilience under dynamic grid disturbances, contributing to more stable and efficient renewable energy integration.

Fig. 16. Harmonic spectra of load current under a sudden load change—(**a**) before the load change under balanced PCC voltage condition, (**b**) before the load change under unbalanced PCC voltage condition, (**c**) after the load change under balanced PCC voltage condition, and (**d**) after the load change under unbalanced PCC voltage condition.
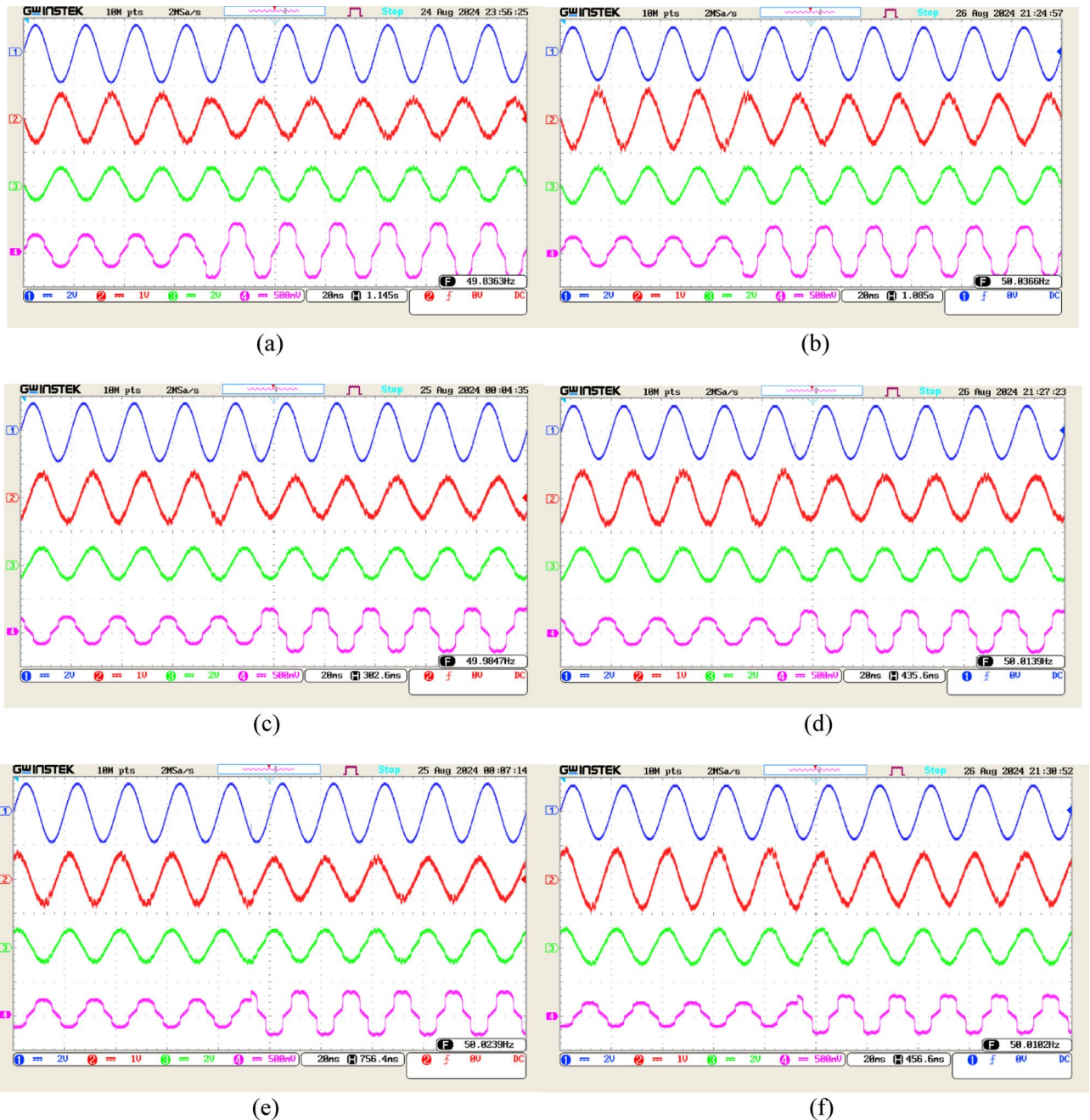
Fig. 17. Real-time performance waveforms of the proposed PV-DSTATCOM under a sudden load change at an irradiance level of 700 W/m^2—(**a**), (**c**), (**e**) performance waveforms under balanced PCC voltage condition for Phase 'a,' Phase 'b,' and Phase 'c,' respectively; (**b**), (**d**), (**f**) performance waveforms under unbalanced PCC voltage condition for Phase 'a,' Phase 'b,' and Phase 'c,' respectively. CH1: Phase 'a' PCC voltage (400 V/div); CH2: source/grid current waveform of respective phase (5A/div); CH3: VSC current waveform of respective phase (10A/div); CH4: load current waveform of respective phase (2.5A/div).

(a)   (b)
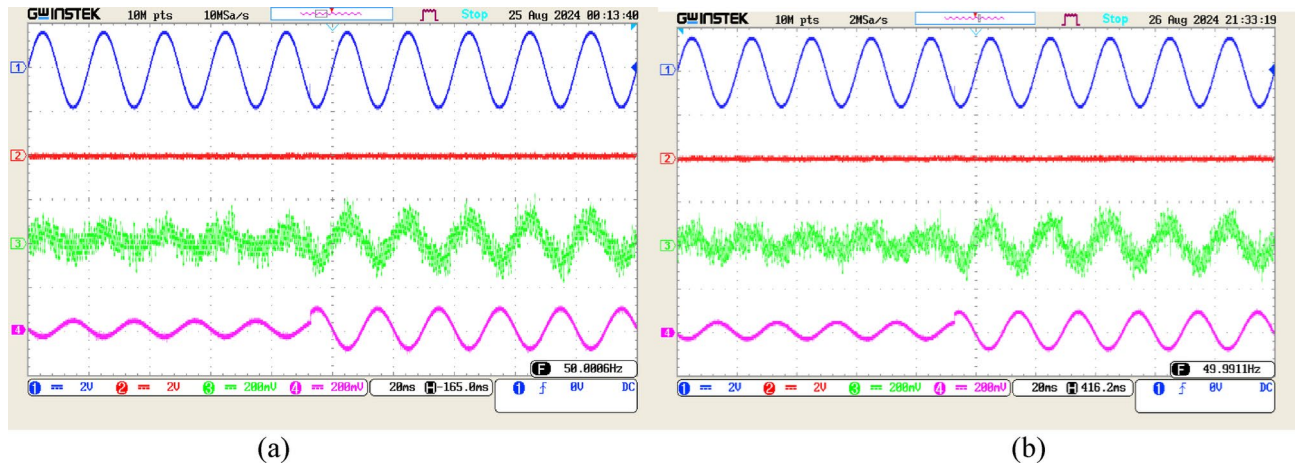
Fig. 18. Real-time waveforms of neutral currents under a sudden load change at an irradiance level of 700 W/m^2—(**a**) neutral current waveforms under balanced PCC voltage condition; (**b**) neutral current waveforms under unbalanced PCC voltage condition. CH1: Phase 'a' PCC voltage (400 V/div); CH2: source/grid neutral current waveform (10A/div); CH3: VSC neutral current waveform (1A/div); CH4: load neutral current waveform (1A/div).
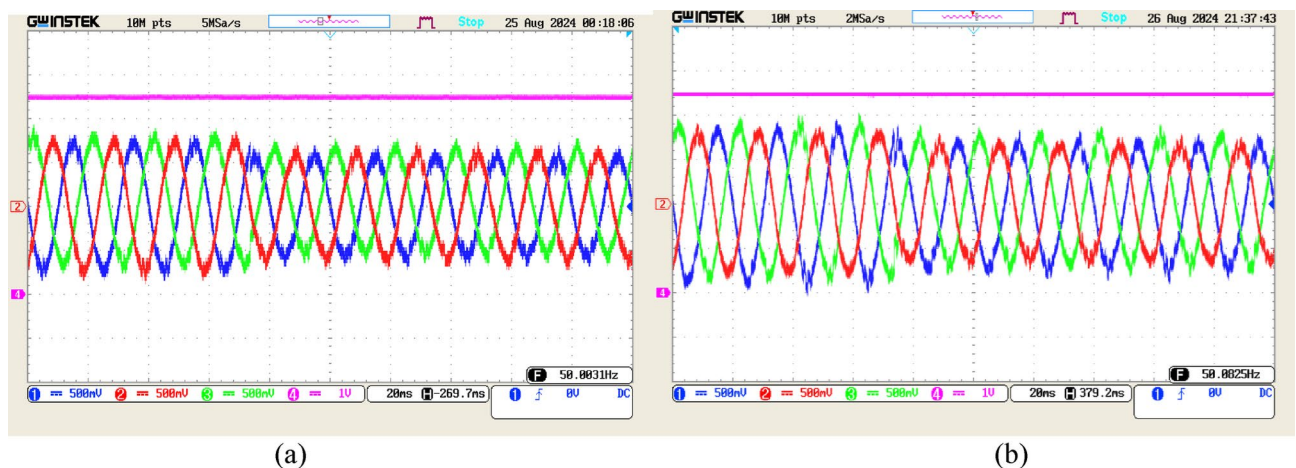

(a)   (b)

Fig. 19. Real-time waveforms of three-phase source/grid currents and DC-link voltage under a sudden load change at an irradiance level of 700 W/m^2—(**a**) waveforms under balanced PCC voltage condition, and (**b**) waveforms under unbalanced PCC voltage condition. CH1 to CH3: source/grid current waveforms (2.5 A/div); CH4: DC-link voltage (200 V/div).

Fig. 20. Harmonic spectra of source/grid current under a sudden load change at an irradiance level of 700 W/m^2—(**a**) before the load change under balanced PCC voltage condition with PV power injection at an irradiance level of 700 W/m^2, (**b**) before the load change under unbalanced PCC voltage condition with PV power injection at an irradiance level of 700 W/m^2, (**c**) after the load change under balanced PCC voltage condition with PV power injection at an irradiance level of 700 W/m^2, and (**d**) after the load change under unbalanced PCC voltage condition with PV power injection at an irradiance level of 700 W/m^2.

Data availability
The data can be requested from the corresponding author.

References
1. Fettah, K. et al. Optimal integration of photovoltaic sources and capacitor banks considering irradiance, temperature, and load changes in electric distribution system. *Sci. Rep.* **15**(1), 2670 (2025).

2. Hashemzadeh, E., Aghamohammadi, M., Asadi, M., Moghaddam, J. Z. & Guerrero, J. M. Secondary control for a D-STATCOM dc-link voltage under capacitance degradation. *IEEE Trans. Power Electron.* **36**(11), 13215–13224 (2021).
3. Dhaundiyal, A. & Atsu, D. The effect of thermo-fluid properties of air on the solar collector system. *Alex. Eng. J.* **61**(4), 2825–2839 (2022).
4. Pandu, S. B. et al. Power quality enhancement in sensitive local distribution grid using interval type-II fuzzy logic controlled DSTATCOM. *IEEE Access* **9**, 59888–59899 (2021).
5. Jayaraman, R., Tummapudi, S., Prakash, R. B. R. & Muni, T. V. Analysis of sliding mode controller based DSTATCOM for power quality improvement in distribution power system. *Mater. Today Proc.* **80**, 3675–3681 (2023).
6. Jahnavi, B., Karanki, S. B. & Kar, P. K. Power quality improvement with D-STATCOM using combined PR and Comb filter-Controller. In *2021 1st International Conference on Power Electronics and Energy (ICPEE)* 1–6 (IEEE, 2021).
7. Gupta, A. Power quality evaluation of photovoltaic grid interfaced cascaded H-bridge nine-level multilevel inverter systems using D-STATCOM and UPQC. *Energy* **238**, 121707 (2022).
8. Chakrabarty, R. & Adda, R. DSTATCOM implementation using reduced switch single DC source cascaded H-bridge multilevel inverter. *Electr. Power Syst. Res.* **199**, 107373 (2021).
9. Singh, B., Jayaprakash, P., Kothari, D. P., Chandra, A. & Al Haddad, K. Comprehensive study of DSTATCOM configurations. *IEEE Trans. Ind. Inform.* **10**(2), 854–870 (2014).
10. Ballestín-Fuertes, J. et al. Four-legs D-STATCOM for current balancing in low-voltage distribution grids. *IEEE Access* **10**, 779–788 (2021).
11. Chenchireddy, K. & Jegathesan, V. Three-leg voltage source converter-based D-STATCOM for power quality improvement in electrical vehicle charging station. In *AI Enabled IoT for Electrification and Connected Transportation* 235–250 (Springer, 2022).
12. Chakraborty, S., Mukhopadhyay, S. & Biswas, S. K. Coordination of D-STATCOM & SVC for dynamic VAR compensation and voltage stabilization of an AC grid interconnected to a DC microgrid. *IEEE Trans. Ind. Appl.* **58**(1), 634–644 (2021).
13. Agrawal, H. P., Bansal, H. O., Kumar, R. & Sisodia, Y. S. HIL investigations on intelligently tuned PV integrated DSTATCOM to enhance power quality. *Arab. J. Sci. Eng.* 1–17 (2022).
14. Joshi, J. et al. Control strategy for current limitation and maximum capacity utilization of grid connected PV inverter under unbalanced grid conditions. *Sci. Rep.* **14**(1), 10118 (2024).
15. Rajan, C. S. & Ebenezer, M. Fuzzy controlled D-STATCOM to improve the PCC voltage profile of a multi-microgrid interconnection scheme. In *Control Applications in Modern Power Systems: Select Proceedings of EPREC 2021* 219–232 (Springer, 2022).
16. Vanam, S. & Gurijala, S. Hybrid energy management system & power compensation of PV & wind integrated grid system with fuzzy based D-STATCOM. In *2022 international conference on electronic systems and intelligent computing (ICESIC)* 206–212 (IEEE, 2022).
17. Sekhar, H. & Manikandan, V. Power quality enhancement using multi-level inverter with UPQC and robust back propagation neural network strategy. *ECS Trans.* **107**(1), 5879 (2022).
18. Chawda, G. S., Shaik, A. G., Mahela, O. P. & Padmanaban, S. Performance improvement of weak grid-connected wind energy system using FLSRF-controlled DSTATCOM. *IEEE Trans. Ind. Electron.* **70**(2), 1565–1575 (2022).
19. Chakraborty, S., Mukhopadhyay, S. & Biswas, S. K. Combined operation of D-STATCOM and low THD SVC in a distribution grid for dynamic VAr compensation and voltage stabilization. In *2020 IEEE International Conference on Power Electronics, Smart Grid and Renewable Energy (PESGRE2020)* 1–6 (IEEE, 2020).
20. Taya, B. B., Ahammad, A. & Jahin, F. I. Total harmonic distortion mitigation and voltage control using distribution static synchronous compensator and hybrid active power filter. *Int. J. Adv. Technol. Eng. Explor.* **11**(114), 624 (2024).
21. Popescu, M., Bitoleanu, A., Linca, M. & Suru, C. V. Improving power quality by a four-wire shunt active power filter: A case study. *Energies* **14**(7), 1951 (2021).
22. Chen, J. H., Tan, K. H. & Lee, Y. D. Intelligent controlled DSTATCOM for power quality enhancement. *Energies* **15**(11), 4017 (2022).
23. Joshi, M. K. & Patel, R. R. A simulation analysis of grid-connected DSTATCOM with PWM voltage control and hysteresis current control for power quality improvement. *Power Electron. Drives* **9**, 220–237 (2024).
24. Kumar, N., Tripathi, S. M. & Govil, V. K. Virtual HIL simulation of grid-tied PV inverter with hysteresis current controller. In *2023 International Conference on Power, Instrumentation, Energy and Control (PIECON)* 1–5 (IEEE, 2023).
25. Dash, A. et al. Performance evaluation of three-phase grid-tied SPV-DSTATCOM with DC-offset compensation under dynamic load condition. *IEEE Access* **9**, 161395–161406 (2021).
26. Patel, N., Gupta, N. & Babu, B. C. Photovoltaic system operation as DSTATCOM for power quality improvement employing active current control. *IET Gener. Transm. Distrib.* **14**(17), 3518–3529 (2020).
27. Nur-E-Alam, M. et al. Optimization of energy management in Malaysian microgrids using fuzzy logic-based EMS scheduling controller. *Sci. Rep.* **15**(1), 995 (2025).
28. Adiche, S. et al. Advanced control strategy for AC microgrids: a hybrid ANN-based adaptive PI controller with droop control and virtual impedance technique. *Sci. Rep.* **14**(1), 31057 (2024).
29. Ahmed, T. et al. Analysis of fractional order sliding mode control in a D-STATCOM integrated power distribution system. *IEEE Access* **9**, 70337–70352 (2021).
30. Fernández, G. et al. Optimal D-STATCOM placement tool for low voltage grids. *Energies* **14**(14), 4212 (2021).
31. Govil, V. K., Sahay, K. & Tripathi, S. M. A survey on DSTATCOM control and power quality improvement techniques. In *2022 1st International Conference on Sustainable Technology for Power and Energy Systems (STPES)* 1–6 (IEEE, 2022).
32. Prashant, Siddiqui, A. S., Sarwar, M., Althobaiti, A. & Ghoneim, S. S. Optimal location and sizing of distributed generators in power system network with power quality enhancement using fuzzy logic controlled D-STATCOM. *Sustainability* **14**(6), 3305 (2022).
33. Satyanarayana, P. V. V. et al. Combined DC-link fed parallel-VSI-based DSTATCOM for power quality improvement of a solar DG integrated system. *Electronics* **12**(3), 505 (2023).
34. Tripathi, S. M., Tiwari, A. N. & Singh, D. Low-voltage ride-through enhancement with the ω and T controls of PMSG in a grid-integrated wind generation system. *IET Gener. Transm. Distrib.* **13**(10), 1979–1988 (2019).
35. Hemalatha, R. & Ramasamy, M. Harmonics extraction scheme for power quality improvement using Chbmli-DSTATCOM module. *Intell. Autom. Soft Comput.* **35**(2), 1505–1525 (2023).
36. Nandagopal, V., Damodhar, T. S., Vijayapriya, P. & Thamilmaran, A. Improving power quality by DSTATCOM based DQ theory with soft computing techniques. *Intell. Autom. Soft Comput.* **36**(2), 1315–1329 (2023).
37. Roy, S., Debnath, A., Tariq, M., Behnamfar, M. & Sarwat, A. Characterizing current THD's dependency on solar irradiance and supraharmonics profiling for a grid-tied photovoltaic power plant. *Sustainability* **15**(2), 1214 (2023).
38. Hepziba, J. R. & Balaji, G. A modified hysteresis current controller with DFCEA for current harmonic mitigation using PV-SHAPF. *J. Chin. Inst. Eng.* **47**(1), 63–80 (2024).
39. Modi, G. & Singh, B. Power quality improvement in solar energy conversion system integrated to weak AC grid. *J. Inst. Eng. India Ser. B* **105**(6), 1511–1526 (2024).
40. Sah, P. & Singh, B. K. Power quality improvement using distribution static synchronous compensator. *Comput. Electr. Eng.* **106**, 108599 (2023).
41. Çelik, D. & Ahmed, H. Enhanced control of superconducting magnetic energy storage integrated UPQC for power quality improvement in EV charging station. *J. Energy Storage* **62**, 106843 (2023).

42. Rastogi, M., Ahmad, A. & Bhat, A. H. Performance investigation of two-level reduced-switch D-STATCOM in grid-tied solar-PV array with stepped P&O MPPT algorithm and modified SRF strategy. *J. King Saud Univ. Eng. Sci.* **35**(6), 393–405 (2023).
43. Ray, P., Ray, P. K. & Marzband, M. Reduced sensor based control of PV-DSTATCOM with switch current limiting scheme. *Energies* **15**(22), 8727 (2022).
44. Tripathi, S. M., Tiwari, A. N. & Singh, D. Optimum design of proportional-integral controllers in grid-integrated PMSG-based wind energy conversion system. *Int. Trans. Electr. Energy Syst.* **26**(5), 1006–1031 (2016).
45. Mishra, A. K. et al. Performance assessment of VSC-based HVDC system in asynchronous grid interconnection: Offline and real-time validation of control design with symmetric optimum PI tuning. *Heliyon* **10**(15), e35624 (2024).

Author contributions

V.K.G. contributes to conceptualization, methodology development, and manuscript drafting. S.M.T. provides supervision, assists in real-time simulation, and contributes to critical revisions. K.S. contributes to supervision and manuscript revision.

Declarations

Competing interests

The authors declare no competing interests.

Additional information

Correspondence and requests for materials should be addressed to V.K.G.

Reprints and permissions information is available at www.nature.com/reprints.

Publisher's note Springer Nature remains neutral with regard to jurisdictional claims in published maps and institutional affiliations.